

An Efficient Receiver Structure for Sweep-Spread-Carrier Underwater Acoustic Links

Leonardo Marchetti and Ruggero Reggiannini

Abstract—In this paper we present an improved receiver architecture for sweep-spread-carrier modulation, a spread-spectrum technique proposed to effectively contrast the effects of time dispersion over multipath propagation channels in underwater acoustic wireless links. The proposed structure is capable to take advantage of the energy received from all propagation paths rather than only from the strongest path, as envisaged in the pioneering paper introducing this modulation technique. A hardware version of the modem was implemented in laboratory and its behavior was assessed and compared, using standard propagation models, to that exhibited by the traditional single-path-based scheme in terms of bit error rate. Results are presented showing that gains of a few decibels can be achieved in signal-to-noise-plus-interference ratio. Issues relevant to carrier/symbol synchronization, channel estimation and sensitivity to Doppler distortion are also addressed.

Index Terms—Multipath propagation, underwater acoustic communications, spread-spectrum, sweep-spread carrier, multiple-branch receiver, rake receiver, maximal ratio combining

I. INTRODUCTION

Underwater acoustic (UWA) communication systems have attracted considerable attention in recent years due to the growing interest for issues related to exploration, surveillance and exploitation of the submarine environment (e.g. [1] - [6]). Most of these applications require some form of wireless communication capability between submerged terminals such as autonomous underwater vehicles (AUVs), platform/mother ships, nodes of underwater networks etc. As is well known, the UWA multipath channel is plagued by several impairments, notably: *i*) severe time dispersion due to the low sound propagation speed with consequent possible distortion of the received waveform, *ii*) for the same reason, amplification of Doppler shifts/rates associated to relative movements of terminals, possibly leading to significant signal distortion for wide signal bandwidths, *iii*) large propagation delays, *iv*) lowpass behavior of the propagation channel caused by sound absorption, leading to strong limitation of bandwidth usage. These factors considerably limit transmission rates and coverage of UWA links in comparison with their electromagnetic radio counterparts and call for the search of more specific and robust signaling schemes. Comprehensive accounts of the above issues along with presentation and discussion of specific transmission schemes can be found e.g. in [3] - [6] and references therein.

A few years ago an unconventional interesting spread-spectrum transmission technique was proposed in [7] and applied to the UWA channel. The basic idea is to employ a sawtooth-frequency-modulated waveform as signal carrier (termed S2C, sweep-spread carrier), with linear frequency ramps, such to facilitate separation at the receiver of the signal replicas collected from the various channel paths. Actually, since these replicas undergo different propagation delays, they are mapped to different positions on the frequency axis when the received signal is downconverted to baseband using a locally-generated copy of the S2C synchronized to the strongest path. A proper design of the signal parameters permits to space the spectral replicas associated with the various paths far enough from one another so as to avoid their overlap. It is therefore possible to single out the strongest path with no interference from the others, thus canceling multipath-induced distortion.

From the pioneering paper [7] to date a number of improvements and variants of the initial scheme of the S2C receiver have been proposed and analyzed. In particular, the patent document [8] presents some conceptual receiver architectures making use of the energy received through multiple propagation paths instead of that from the strongest path only. Specifically, in [8, Fig. 19] a receiver block diagram is sketched wherein two signal replicas collected from different paths are processed by parallel receiver branches, and their individual phases and relative delay are corrected before the waveforms are applied to a block identified as “combined demodulator”. The document however does not specify how the cited phases and delays are estimated, nor does it provide details about the operation of the demodulator. Furthermore, it was out of the scope of [8] to analyze and compare the performance of the above architectures. Additional related qualitative and quantitative results can be found in [9]–[11] addressing the impact of imperfect separation (and consequent onset of mutual interference) of the signal replicas being processed by the receiver branches on the estimation of their individual phases and relative delays, needed for combined demodulation.

In this paper we make some steps ahead, by proposing and discussing a further implementation of the S2C receiver which integrates the schemes presented in the above references. As in [8], we consider an advanced receiver structure capable of enhancing the power efficiency of the scheme in [7] through exploitation of the energy received from multiple nonnegligible acoustic paths rather than only from the strongest path.

This goal can be achieved by first identifying the paths of significant level, then performing extraction and parallel elaboration for each of them and finally combining the decision

metrics from each processing branch. A noteworthy difference with respect to the schemes enumerated in [8] is that here we resort to an optimal approach to combine the branch outputs. The resulting multiple-branch receiver architecture is similar to that used for the reception of direct-sequence spread-spectrum (DS-SS) signals over time-dispersive wireless links, known as “rake receiver” [12, Chapt. 13.5], but the context considered here is different as we have now to face the peculiar issues related to the unconventional format of the S2C waveform, involving for instance a different mechanism through which the received signal replicas interfere with each other after the despreading/demodulation stage.

A further contribution of this paper is to propose and assess a synchronization technique for the joint recovery of carrier and clock references for each of the signal replicas processed by the receiver. Its accuracy is provided in terms of root-mean-square synchronization errors.

A real-time hardware version of the modem, complete of synchronization functions, was implemented in laboratory and its behavior was assessed over standard UWA channel emulators and compared to that exhibited by the traditional strongest-path-based scheme in terms of bit error rate (BER) vs. signal-to-noise ratio. Moreover, the sensitivity of the multiple-branch receiver to residual Doppler distortion is assessed and compared to that exhibited by the single-branch scheme.

The paper is organized as follows. In Section II we briefly review signal and channel models, while in Section III we illustrate the modem architecture with emphasis on the multiple-branch receiver section. Section IV discusses the algorithms for channel estimation and carrier/timing synchronization. Section V defines conditions for path resolvability, provides details on how the received waveform is processed in the multiple-branch structure and also describes the system hardware implementation. Section VI presents simulation setup and results. Conclusions are finally drawn in Section VII.

II. SIGNAL AND CHANNEL MODELS

Now we briefly review the S2C signal format paralleling the presentation in [7], which the reader is referred to for further details. We assume information is transmitted in the form of data packets, each starting with a preamble of P known pilot symbols, to be employed for carrier and symbol synchronization/tracking, followed by a payload of D symbols. Letting T denote the symbol spacing, the packet length is $T_B = (P+D)T$. The number of packets and the instants for their transmission depend on both the amount of information to be transferred and the specific link protocols, and are not of interest for the paper scope.

Focusing then on a generic packet at the transmitter side, the signal at baseband, prior to spectral expansion and frequency upconversion, is a conventional linearly-modulated waveform

$$s(t) = \sum_{i=0}^{P+D-1} a_i g(t - iT) \quad (1)$$

where $\mathbf{a} \triangleq [a_0, \dots, a_{P+D-1}]^T$ denotes the vector of

(differentially-encoded) QPSK symbols in the packet, and $g(t)$ is a root-raised-cosine pulse with roll-off factor α . In particular, the pseudo-random sequence $\mathbf{p} \triangleq [p_0, \dots, p_{P-1}]^T$ of pilot symbols is common to all packets, while the sequence $\mathbf{d} \triangleq [d_0, \dots, d_{D-1}]^T$ represents a specific data segment.

After spectral spreading and frequency upconversion, the bandpass signal to be fed to the acoustic projector can be written as

$$x(t) = \Re\{s(t)c(t)\} \quad (2)$$

$c(t)$ denoting a frequency-modulated carrier achieving both frequency conversion and bandwidth expansion, as follows

$$c(t) = \exp\{j2\pi [f_L \tau(t) + m\tau^2(t)]\} \quad (3)$$

where $\tau(t)$ is a sawtooth-shaped periodic sweep function, with period T_{sw}

$$\tau(t) = t - \left\lfloor \frac{t}{T_{sw}} \right\rfloor T_{sw} \quad (4)$$

$\lfloor z \rfloor$ being the largest integer not exceeding z . In (3), f_L represents the lower limit of the frequency ramps, while $2m$ is the ramp slope. The instantaneous carrier frequency during a ramp is proportional to the derivative of the argument of the exponential in (3)

$$f_i(t) = f_L + 2m \left(t - \left\lfloor \frac{t}{T_{sw}} \right\rfloor T_{sw} \right). \quad (5)$$

It follows that the upper frequency limit is $f_H = f_L + 2mT_{sw}$. The limits f_L and f_H , along with the sweep interval T_{sw} , usually taken an integer multiple of the symbol spacing, are key design parameters as they define the slope $2m = \frac{f_H - f_L}{T_{sw}}$ of the ramps and characterize the ability of the receiver to resolve the multipath channel structure (i.e., to separate the signal replicas arriving from the various paths).

After spreading and frequency upconversion, the signal bandwidth amounts to approximately $B \approx f_H - f_L$, i.e., it is expanded by a factor (*spreading factor*)

$$\mathcal{M} \triangleq \frac{f_H - f_L}{T} \quad (6)$$

with respect to a conventional narrowband signal, \mathcal{M} usually being much greater than unity.

A general expression of the multipath time-varying UWA channel impulse response is as follows

$$r_c(t, t_0) = \sum_{k=0}^{N_p(t_0)-1} h_k(t_0) \delta[t - t_0 - \tau_k(t_0)] \quad (7)$$

where $N_p(t_0)$ is the number of (nonnegligible-level) paths and $h_k(t_0)$, $\tau_k(t_0)$ are the (complex-valued) gain and delay of the k -th path, respectively, all evaluated at the instant of application of the impulse $t = t_0$. In the following we assume that the channel variations are negligible in a time span comparable to the packet length, so that the information about the channel parameters in (7), estimated from the packet preamble, can be considered reliable throughout the whole payload segment. This is not a severe constraint since transmission on the UWA link is normally preceded by a procedure of adjustment of the transmission parameters to the

channel conditions. Accordingly, the dependence of the model in (7) on t_0 can be dropped and all channel parameters can be regarded as random variables instead of random processes. Therefore the received waveform can be written as

$$y(t) = \sum_{k=0}^{N_p-1} y_k(t) + w(t) \quad (8)$$

where $w(t)$ is AWGN of double-sided spectral density $N_0/2$, accounting for both external and internal disturbance sources affecting the receiver, and $y_k(t)$ is the waveform received through the k -th path, i.e., scaled by the coefficient h_k and delayed by τ_k

$$y_k(t) = \Re\{h_k s(t - \tau_k) c(t - \tau_k)\}. \quad (9)$$

We observe that the main purpose of this paper is to propose a multiple-branch receiver architecture alternative to the schemes presented in [8] and to demonstrate that it may lead to a significant gain in power efficiency in comparison with the basic scheme in [7]. In this perspective we felt it adequate to assume the relatively simple path model (9) and to limit the receiver functions to those strictly required to pursue the above goal. In particular, we decided not to tackle in detail the issues related to time variability and Doppler distortion, that in a practical receiver must be dealt with at an early stage of processing of the incoming packets. This approach is in line with that followed in [7]. However in Section VI we provide results about the sensitivity of multiple-branch and single-branch receivers to residual Doppler errors on each receiver branch.

III. MODEM ARCHITECTURE

A functional block diagram of the S2C modem is depicted in Fig. 1. The transmitter section consists of a standard S2C modulator similar to that discussed in [7]. The information bits are fed to a BCH encoder followed by a DQPSK symbol mapper. The resulting symbol sequence is used to build the data packet (function not detailed in the figure) that is passed through the shaping filter and finally applied to the S2C frequency upconverter.

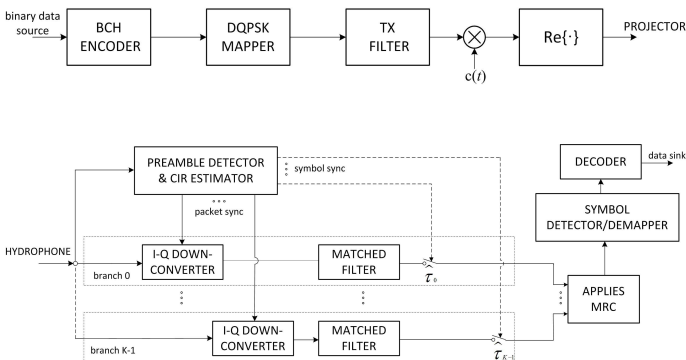


Fig. 1. Modem architecture.

The receiving section includes a block for preamble detection and channel impulse response (CIR) estimation, whose task is to identify, for each packet, the times of arrival of the preamble from the K strongest paths and also to estimate

the (complex-valued) gains of these paths. This leads to the receiver architecture indicated in Fig. 1, wherein each of the K parallel branches is used to process the signal received from a single path. Specifically, with regard to the k -th branch, the input is applied to an in-phase and quadrature converter which multiplies it by a replica of the S2C waveform synchronized with that received from the k -th path. In this way the signal spectrum relative to that path is despread and exactly converted to baseband, while subsequent matched filtering removes interference from the other paths provided that their spectra do not overlap the “good” spectrum at baseband, i.e., their differential propagation delays with respect to the k -th path are sufficiently large. The design criteria for this condition to hold true are discussed in Section V.

As next step, the matched filter output is sampled at symbol rate at the instants $iT + \hat{\tau}_k$, where $\hat{\tau}_k$ is an estimate of τ_k provided by the CIR estimator. Assuming exact ISI cancellation, from (1) and (8)-(9) the generic sample takes on the form

$$v_{k,i} = h_k a_i + w_{k,i}, \quad i = 0, \dots, D - 1 \quad (10)$$

the term $w_{k,i}$ denoting the noise sample generated from $w(t)$ in (8) after the above processing steps through the k -th branch.

Finally, the K samples relevant to the symbol a_i are combined according to the maximal ratio combining (MRC) criterion [12] prior to being fed to the symbol detector and the decoder. With regard to the MRC block, we observe that a sufficient condition for the noise terms $\{w_{k,i}\}_{k=0}^{K-1}$ to be mutually uncorrelated is that the differential delays between the various paths obey the same conditions allowing separation of the respective signal replicas, to be established in Section V. Indeed, the spectra of two incoming signal replicas can be separated by the despreader/demodulator on condition that their relative delay and the slope of the frequency ramps are sufficiently large. When this happens, the noise processes at the output of the matched filters on the respective receiver branches occur as well to be generated from the demodulation of frequently non-overlapping segments of the broadband input noise, and are therefore uncorrelated, this independently of the wideband noise spectral shape.

Finally it is noted that when $K = 1$ the receiver structure reduces to that discussed in [7] where only the strongest path is processed.

IV. TIMING AND CHANNEL ESTIMATION

As mentioned earlier, the first operation to be accomplished at the receiver site is estimation of the timing of arrival of the signal replicas propagating along the channel paths. This permits to synchronize locally generated copies of the S2C waveform with those associated with the K strongest paths and then proceed to separate the signal replicas received from these paths. Another important related task is estimation of the complex-valued channel gains so as to identify the strongest paths and correctly apply the MRC technique.

Both the above operations are carried out by means of a correlator, as is now briefly outlined. Let $s_P(t)$ denote the baseband continuous-time version of the preamble separated

from the payload, as follows

$$s_P(t) = \sum_{i=0}^{P-1} p_i g(t - iT) \quad (11)$$

and also let

$$x_T(t) = s_P(t)c(t) \quad (12)$$

denote the complex-valued bandpass version of the preamble incorporating both frequency upconversion and bandwidth expansion. It is noted from (2) that the real part of (12) represents the transmitted preamble.

Using for simplicity continuous-time notation, the task of the correlator is to calculate the inner product between the template function (12) and a newly received segment of the input waveform, and then take its squared modulus, as follows

$$z(t) = |r(t)|^2, \quad t \in \mathcal{T} \quad (13)$$

where

$$r(t) = \int_0^{T_P} y(t + \tau - T_P) x_T^*(\tau) d\tau, \quad (14)$$

\mathcal{T} is a time interval in which the preamble is expected to be received and $T_P = PT$ is the preamble length. The receiver stores the functions (13)-(14) in memory along with the raw received waveform $y(t)$ for subsequent processing.

When path delays are sufficiently spaced from one another and the signal-to-noise-plus-interference ratio on the paths is high, the squared correlation $z(t)$ exhibits a definite peak in correspondence of each of the delays $\{\tau_k\}$. This can be verified observing that the width of the correlation peaks is approximately equal to the inverse of the template waveform to be detected. Figure 2 shows an example of such a function, obtained from the set of parameters specified in Section VI. Here the symbol spacing is 1.5 ms and the template signal bandwidth is approximately equal to the difference between the upper and lower limits of the frequency ramp, i.e., 16 kHz. Thus the correlation peaks have a width in the order of 0.1 ms, which represents a measure of the delay resolution capability of the correlator. In the time scale of Fig. 2, covering several tens of symbols, and in comparison with typical values of differential delays (see Tab. II in Section VI), these peaks are very narrow and easy detectable at the operating signal-to-noise ratios.

More specifically, assuming for a moment that the receiver is driven by a single noiseless signal replica received from the k -th path (see (9)), it is found that (13) peaks at the instant $T_P + \tau_k$, and the corresponding value for the inner product (14) is

$$r(T_P + \tau_k) = \frac{E_{S_P}}{2} h_k, \quad (15)$$

where $E_{S_P} = \int_0^{T_P} |s_P(\tau)|^2 d\tau$ is the energy of $s_P(t)$. From (15) it is seen that at the instant where the squared correlation peaks the inner product yields a value proportional to the path gain h_k , while the squared peak level is proportional to $|h_k|^2$. Therefore (14) provides all information necessary for path sorting, ramp synchronization and implementation of the MRC detector.

Collecting the above, once correlation (13) has been cal-

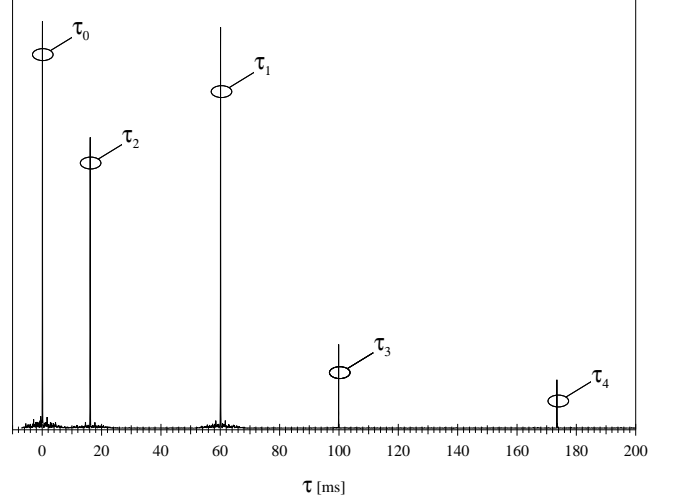


Fig. 2. A sample correlation function (square modulus). The vertical scale is arbitrary. The number of paths is $N_p = 5$, and the other system parameters are specified in Section VI.

culated, a maximum search procedure must be initiated to obtain an estimate of the delay associated to each preamble replica arriving at the receiver. Of course the procedure must be capable to detect “good” correlation peaks against false peaks produced by noise and possibly by sidelobes associated to good peaks. This can be achieved through a simple approach consisting of the following steps. First, the noise level must be estimated by the receiver during the silent periods prior to transmissions or between the transmission of two consecutive messages. Knowledge of the noise level along with the correlator parameters allows to infer the noise-only statistics of the correlator output, and to fix a threshold λ yielding a desired tradeoff between false and missed detection probabilities, with reference to limit conditions characterized by the least operating signal-to-noise ratios, e.g. when the distance between terminals is at the limit of coverage. As next step, the search algorithm looks for the peaks exceeding the threshold and tries to classify them according to their strength and differential delays. This operation is aimed at identifying the “best” paths, i.e., those with largest level and with sufficient delay from one another so as to be easily separable by the despreading/demodulation block. The algorithm starts by estimating the delay associated to the strongest replica (assumed relevant to the path of index zero), as follows

$$\hat{\tau}_0 = \arg \max_{\substack{z(t) > \lambda \\ t \in \mathcal{T}}} z(t). \quad (16)$$

The delays associated to the other $N_p - 1$ paths of significant gain are identified by looking for the other local maxima of $z(t)$, using the following iterative approach

$$\hat{\tau}_i = \arg \max_{\substack{z(t) > \lambda \\ t \in \mathcal{T} \\ t \notin \mathcal{I}_i}} z(t), \quad i = 1, 2, \dots, N_p - 1 \quad (17)$$

where \mathcal{I}_i denotes a set of subintervals of \mathcal{T} centred around the values of delay already identified through step $i - 1$, that

must be excluded from the search at the current step i , i.e.

$$\mathcal{I}_i = \{(\hat{\tau}_0 - T_{cor}, \hat{\tau}_0 + T_{cor}) \cup \dots \cup (\hat{\tau}_{i-1} - T_{cor}, \hat{\tau}_{i-1} + T_{cor})\}. \quad (18)$$

In this way the N_p strongest paths are orderly identified along with their delays. However, problems may arise at this stage if the peaks are spaced too tightly, i.e., if the corresponding relative path delays are too close to one another. As noted earlier, the width of the correlation peaks is given approximately by the inverse of the template signal bandwidth. This provides a measure of the delay resolution capability of the correlator, inasmuch as peaks that are spaced less than this measure cannot be distinguished. A further aspect to be taken into account is the presence of sidelobes around the correlation peaks in (13), that for very strong signal level could exceed the threshold and be misdetected as additional independent peaks. To avoid the latter type of error it is convenient that the length $2T_{cor}$ of the windows centered on the correlation peaks be selected large enough to include a few sidelobes as well, at the cost of accepting a further slight degradation in the detector resolution properties. With reference to the set of parameters in the example of Section VI, the parameter $2T_{cor}$ can be fixed at 1 ms (covering the main correlation lobe plus a few sidelobes on each side), which is still far smaller than the channel delay spread in a typical scenario.

When the above procedure of multiple path detection and classification is over, the receiver must select a number $K \leq N_p$ of paths to be processed in its K branches. A reasonable criterion is to select the strongest K paths, but some of these could be discarded at this stage if their differential delay is not sufficient to ensure adequate separation of their spectra after despreading/demodulation.

In addition to estimating the delay of the main usable paths of the UWA channel, the receiver must proceed to evaluate the relevant complex-valued path gains in view of their usage within the MRC block (see Fig. 1). As noted earlier, these gains are provided by (15) as a by-product of the same correlation algorithm employed for path delay estimation.

V. DESIGN ISSUES AND HARDWARE IMPLEMENTATION

A. Conditions for path resolvability

Recalling the discussions in Sections II and III, for the K -branch receiver of Fig. 1 to work properly it is required that, for each branch, the signal spectrum converted to baseband does not collide with the spectra of the signal replicas being processed by the other branches. This allows the signal at baseband to be extracted by means of a simple (lowpass) matched filter. For these conditions to be met, it is necessary that the differential delays between all pairs of paths do not drop below a certain threshold. A further constraint is that the maximum differential delay must not exceed T_{sw} to avoid ambiguities in delay estimation.

More specifically, with no loss of generality we can treat $\{\tau_k\}_{k=0}^{K-1}$ as differential delays with respect to τ_0 , arranged in nondecreasing order, i.e., we set $\tau_0 = 0 \leq \tau_1 \leq \dots \leq \tau_{K-1}$. Then the constraints to be put on these differential delays are as follows (see also [7])

$$\begin{cases} 2m\delta\tau_{min} \geq \frac{1+\alpha}{T} \\ -2m\delta\tau_{max} + f_H - f_L \geq \frac{1+\alpha}{T} \end{cases} \quad (19)$$

where $\delta\tau_{min} = \min_{0 \leq i, j \leq K-1} |\tau_i - \tau_j|$, $i \neq j$, is the minimum (absolute) differential path delay and $\delta\tau_{max} = \max_{0 \leq i, j \leq K-1} |\tau_i - \tau_j| = \tau_{K-1}$, $i \neq j$, is the maximum differential path delay, or channel time dispersion. Using (6) in (19) yields

$$\begin{cases} T_{sw} \leq \mathcal{M}\delta\tau_{min} \\ T_{sw} \geq \frac{\mathcal{M}}{\mathcal{M}-1}\delta\tau_{max} \end{cases} \quad (20)$$

For the existence of values of T_{sw} satisfying both the above conditions it is required that

$$1 \leq \frac{\delta\tau_{max}}{\delta\tau_{min}} \leq \mathcal{M} - 1. \quad (21)$$

The first inequality in (20) sets a lower limit to the absolute difference between the arrival times of any two signal replicas. When the difference exceeds this limit, the receiver is able to accurately resolve the channel multipath structure. Otherwise, when two received replicas are spaced too closely, after despreading they will overlap in the frequency domain, thus preventing their exact separation. On the other hand, the second inequality in (20) puts an upper limit to the differential path delays, approximately equal to T_{sw} when \mathcal{M} is large. Actually, a signal replica delayed more than T_{sw} with respect to the one traveling on the shortest path would generate a timing estimate affected by an ambiguity equal to an integer multiple of T_{sw} that could not be detected and recovered, with a negative impact on the MRC algorithm.

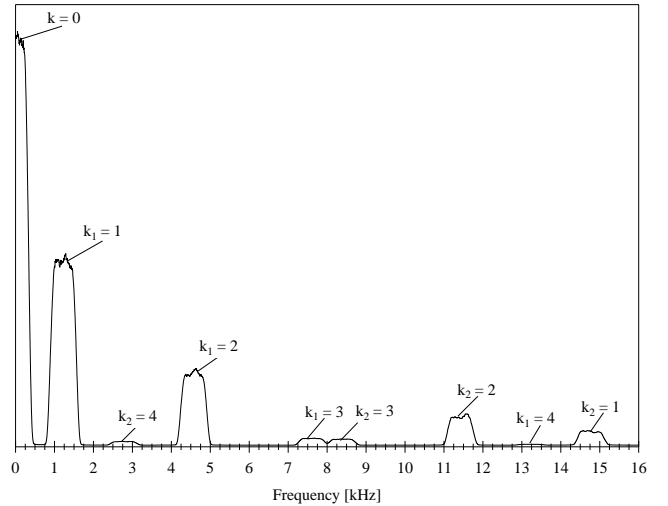


Fig. 3. Power spectral density of the received signal after downconversion/despreading of the strongest path ($k = 0$). The vertical scale is arbitrary. The system parameters are the same as in Fig. 2 and are specified in Section VI.

Figure 3 shows a realization of power spectral density of the received signal after downconversion/despreading for a five-ray scenario, assuming that downconversion is carried out for the strongest path. Transmission parameters are the same as in the example of Fig. 2. Inspection of the figure reveals that in this case all paths are resolvable (apart from a marginal overlap

of two small spectral replicas located midway on the frequency axis), and in particular the useful signal (whose spectrum lies around the origin) can be recovered by means of a lowpass filter, without (or with negligible) interference from the other replicas. The latter signal components, carrying useful power as well, can in turn be extracted by multiplication of the received waveform by properly delayed replicas of $c(t)$ followed by lowpass filtering, as illustrated in Section III. More specifically, from Fig. 3 it is seen that, in addition to the signal spectrum centered on the origin, there are eight other spectral replicas generated by the paths with delays τ_1, τ_2, τ_3 and τ_4 . Indeed, recalling (19) and the ensuing discussion, the k -th path gives rise to two spectral components (identified with the indices k_1 and k_2 in Fig. 3), centered around the frequencies $2m\tau_k$ and $f_H - f_L - 2m\tau_k$, $k = 1, 2, 3, 4$, respectively. The actual values of these frequencies are specified in Tab. II.

B. Merging branch outputs

As mentioned earlier, the receiver is made up of K parallel branches, designed to jointly extract and elaborate up to K replicas of the signal received from the multipath UWA channel. The k -th branch proceeds to despread/downconvert the received signal through its multiplication by $c(t - \hat{\tau}_k)$, as described in Section IV, where $\hat{\tau}_k$ is an estimate of the propagation delay on the k -th path. Assuming error-free delay estimates and exact resolvability of the signal on all branches according to the criteria identified in Section V-A, the sampled output of the k -th branch takes on the form (10). All branch outputs are then combined according to the MRC optimality criterion, as follows

$$q_i = \sum_{k=0}^{K-1} \hat{h}_k^* v_{k,i} \quad (22)$$

where \hat{h}_k is the estimate of the k -th path gain. The sequence of samples (22) is then fed to the decoder/data detector for further processing.

As mentioned in the Introduction, the above approach is reminiscent of that employed in the so-called ‘‘rake receiver’’ proposed for conventional DS-SS modulations [12], even though the context here is different from that envisaged in typical electromagnetic wireless links. Actually the mechanism generating mutual interference between two replicas of the signal arriving from different paths is not the same in DS-SS and S2C. In the case of a DS-SS system, the spreading code is normally designed so as to be self-uncorrelated, i.e., it is sufficient to shift two signal replicas by just one code chip, and the mutual interference, after the despreading and matched filtering stages, is reduced by approximately the spreading factor. This interference does not decrease further if the delay between replicas grows. In the frequency domain, the presence of the interfering signal results in a small increase in the (approximately white) spectral level of noise and interference. Conversely in the case of a S2C system, achievement of orthogonality between the signal replicas relies on the ability of the frequency ramp to separate their spectra, and in turn this depends jointly on the relative time delay between the paths and on the slope of the ramp itself. It follows that, due to

the presence of the out-of-band ripple in the baseband signal spectrum and the rolloff region (with sidelobes as well) of the matched filter responses, the amount of mutual interference depends on the frequency-domain distance between the spectra after despreading/demodulation: the larger this distance, i.e., the larger the relative delay between the two replicas and/or the ramp slope, the lower will be the interference, and viceversa. Furthermore, the demodulation process in the S2C system is affected by occasional frequency jumps of the interfering replicas (see e.g. Fig. 4 in [7]), representing a specific form of disturbance that is absent in the DS-SS context.

However, assuming the K paths can be resolved, we can borrow from the rake receiver the expression of the asymptotic gain in power efficiency

$$G_R = \frac{\sum_{k=0}^{K-1} E\{|h_k|^2\}}{E\{|h_0|^2\}}, \quad (23)$$

$E\{\cdot\}$ denoting statistical expectation, that can be achieved with respect to the receiver operating on the single path of gain h_0 . This result has been confirmed by simulations (Section VI).

C. Hardware implementation

Now we briefly present our real-time implementation of the modem architecture discussed in the foregoing sections. The testbed is based on *National Instruments* (NI) hardware [13], controlled by *LabView* (LV) applications. Specifically, we used the chassis NI PXIe-1085 equipped with the controller NI PXIe-8135 and the data acquisition board NI PXIe-6361. The entire system is controlled by a LV-based code that exploits the built-in functions provided in the *RF Communications* toolkit. The transmitter and receiver sections of the modem were both entirely implemented in hardware. Figure 4 shows the complete test bench used for the modem implementation, composed by the controller board within the chassis, a PC running *ad-hoc* LV application software and also a spectrum analyzer.

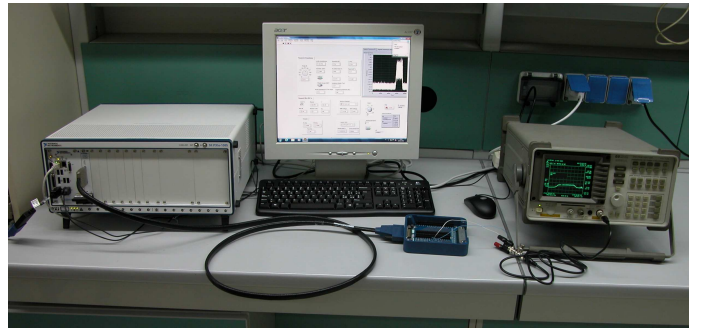


Fig. 4. Test bench: NI chassis hosting controller and data acquisition board, PC with LabView, spectrum analyzer.

VI. SIMULATION RESULTS

The transmission architecture in Fig. 1 was implemented and assessed using the hardware testbed described in Section V-C, in conjunction with the software package *Bellhop* [14], a popular open-source simulator of the UWA environment. In particular, this simulator permits to identify both the coherent

and non-coherent channel profile, i.e., for a fixed number of paths, their complex-valued (modulus and phase) gains, or simply their RMS values, vs. propagation delay, to be associated to an arbitrary UWA operating scenario.

For simplicity, in the following we limit our consideration to a single scenario, characterized by shallow water (130 m) with sound-speed profile vs. depth typical of the summer period and plotted in the left section of Fig. 5. The values assumed for the main geometric and acoustic parameters of the UWA scenario are summarized in Tab. I, while Fig. 6 provides a pictorial representation of the link geometry. In the right section of Fig. 5 we also show the curves produced by the Bellhop ray tracing tool, that can be used to calculate the channel power-delay profile.

TX depth	20 m
RX depth	80 m
Horizontal distance	500 m
Bottom type	gravel
Bottom depth	130 m
Surface (for reflection properties only)	sea state 0
Sound-speed profile	see Fig. 5
Center frequency	26 kHz
TX launching angles	$0^\circ : +180^\circ$

TABLE I
MAIN ACOUSTIC AND GEOMETRIC PARAMETERS OF THE UWA SCENARIO.

Using the ambient parameters of Tab. I and the *Bellhop* tool it is possible to create a multipath propagation model with a fixed number of paths. Here we limit our attention to the strongest first five paths (direct plus four experiencing single or multiple reflections from the surface and/or the bottom). We note that simulations carried out with a larger number of paths (up to 15) showed negligible deviations from the results obtained with 5 paths.

With reference to the link geometry of Fig. 6, the resulting power-delay profile is visible in Tab. II. From *Bellhop* it can be seen that the power associated to these five paths amounts to more than 96% of the total received power in the above scenario. For simplicity the powers associated to the paths in Tab. II are normalized so that they sum up to unity. Moreover, the attenuation over the direct path is assumed deterministic, while the other path coefficients are modeled as independent identically-distributed circular Gaussian variables with zero mean and normalized powers given in column 2, rows 1-4 of Tab. II. As to the spectral shifts specified in the last column of Tab. II, their meaning is defined at the end of Section V-A.

Finally, the physical layer communications parameters used throughout the trials are specified in Tab. III.

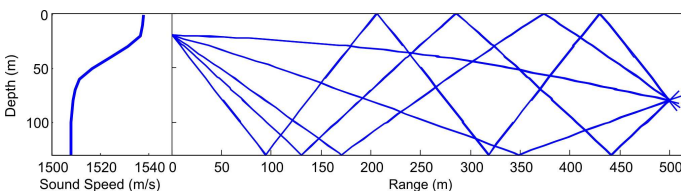


Fig. 5. Ray tracing produced by *Bellhop*.

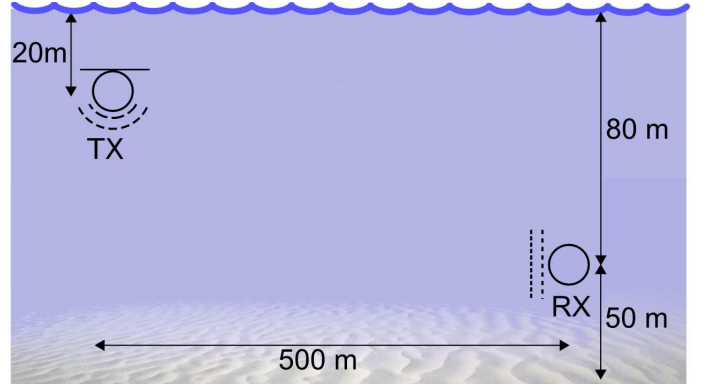


Fig. 6. Geometry of the UWA link.

Path	Normalized power	Relative delay [ms]	Spectral shifts [kHz]
0	0.388	0	0
1	0.380	16.11	1.227, 14.773
2	0.198	60.04	4.575, 11.425
3	0.025	99.84	7.607, 8.393
4	0.009	173.49	13.218, 2.782

TABLE II
POWER-DELAY PROFILE FOR THE 5-PATH CHANNEL.

The five-path channel defined by Tab. II was implemented on the NI testbed using the previously described model. In particular, for every channel realization the receiver input is generated by combining five versions of the transmitted waveform, each with a different delay and attenuation according to the statistics specified in Tab. II and remarks thereof. The signal-to noise ratio (SNR), defined as the ratio between the average energy per symbol received through *all* considered paths to the noise power spectral density, is varied by injecting AWGN with variable spectral level.

Specifically, our purpose here is to compare the performance of the conventional receiver in [7] with that achievable by the multiple-branch parallel structure in Fig. 1 where we assume $K = 3$. This seems a reasonable choice to achieve a substantial gain without exceeding in receiver complexity. To this aim, we observe that, from (23) and from the values in the first three rows of Tab. II, corresponding to the three strongest paths, the maximum expected gain of the three-branch receiver is $G_R \approx 3.96$ dB. This margin seems to be actually achievable in view of the fact that the parameters $\delta\tau_{min}$ and $\delta\tau_{max}$ do largely satisfy condition (21): $\delta\tau_{max}/\delta\tau_{min} \approx 10.77 \ll \mathcal{M} - 1$. Further to be noted, since the three considered signal components can be exactly separated by the receiver, the relative phase rotations associated to the path gains are immaterial, and the receiver performance is only affected by the non-coherent power-delay profile.

Figure 7 shows plots of the bit error rate (BER) vs. SNR obtained for uncoded transmission assuming error-free channel estimation and carrier/symbol synchronization in all receiver branches. The plots were obtained from Monte Carlo simulations over a large number of channel and symbol realizations. The two curves of BER are relevant to the conventional single-branch ($K = 1$) and to the three-branch ($K = 3$) receivers. It

T_{sw}	210 ms
T_P	$2T_{sw}$
\mathcal{M}	20
α	0.2
Symbol spacing	1.5 ms
Payload length	1024 symbols
Modulation	DQPSK
Codec	uncoded, BCH (1431, 2047)
Data rate (payload)	1333 bit/s, 931 bit/s
f_L	18 kHz
f_H	34 kHz
T_{cor}	$8/(f_H - f_L)$

TABLE III
PHYSICAL LAYER PARAMETERS.

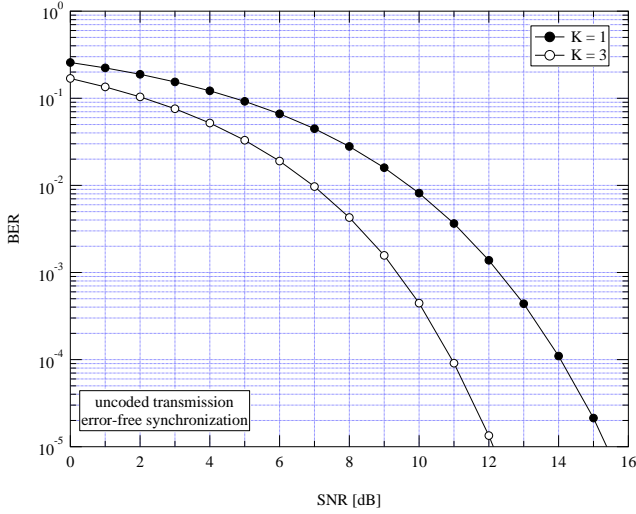


Fig. 7. BER vs SNR, uncoded transmission, 5-path channel, single-branch and three-branch receivers.

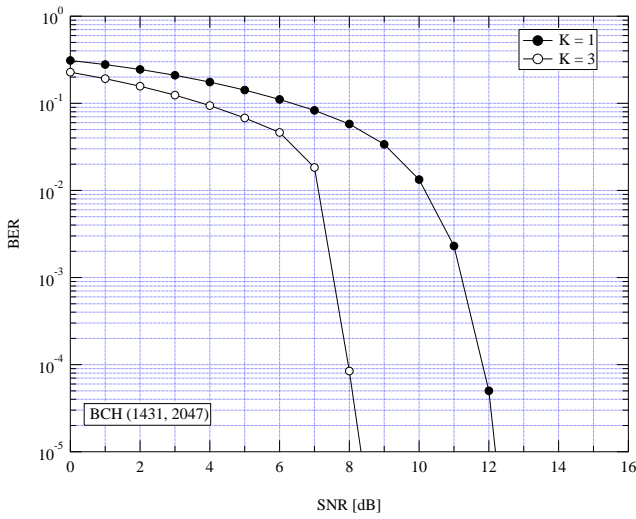


Fig. 8. BER vs SNR, coded transmission, 5-path channel, single-branch and three-branch receivers.

is observed that the latter scheme asymptotically outperforms the former by around 3.3 dB, very close to the asymptotic gain G_R .

Figure 8 shows curves of BER vs. SNR for the same single-branch and three-branch receivers, obtained in the more realistic situation in which the transmitter employs a BCH encoder, with coding rate $r = 1431/2047 \simeq 0.7$, and the receiver actually incorporates the channel estimator and the carrier/symbol synchronizer discussed in Section IV. The benefit in terms of SNR gain provided by the multiple-branch receiving structure is still apparent. For example, at $\text{BER} = 10^{-5}$ this gain is around the asymptotic value of 4 dB, while the advantage provided by the BCH encoder with respect to uncoded transmission (curves in Fig. 7) is more than 3 dB.

In passing, we also assessed the receiver behavior with the MRC replaced by the simpler scheme known as equal gain combiner (EGC) [12] where the combination rule is as in (22) with \hat{h}_k^* replaced by $\hat{h}_k^*/|\hat{h}_k|$. This led to a negligible performance degradation (results not shown) with respect to MRC in the scenario of Tab. II, as is to be expected when there is no definite predominant path, as in links where the transmit and receive transducers are weakly directive, and thus the strength of the surface-reflected (and possibly bottom-reflected) path is comparable to that of the direct path. Conversely when the path levels are strongly unbalanced the MRC approach is likely to exhibit an edge.

It is now appropriate to briefly discuss the performance of the path delay estimator which, as we have seen, plays an important role for synchronization of the despreading waveforms in the multiple-branch receiver, as well as for symbol timing recovery.

As discussed in Section IV, the delay is estimated by determining the instant at which the squared correlation (13) exhibits a peak. Of course, a necessary condition to get an accurate estimate is that the sampling rate at the receiver input be adequately high. The results presented here are obtained using a sampling rate of 100 kHz, a condition which, recalling the data of Tab. III, corresponds to taking 100 samples per symbol and slightly more than 3 samples per cycle at the highest instantaneous frequency f_H of the waveform $c(t)$. In addition, to further improve the accuracy of the above estimator, we resorted to a parabolic interpolator operating on the highest sample of the squared correlation and on the adjacent two. This scheme was considered satisfactory insofar as a further increase of the sampling rate was observed not to entail any additional gain in terms of root mean square estimation error (RMSEE).

Figure 9 shows plots of RMSEE affecting the delay estimates for the three strongest paths of the five-path scenario defined by Tabs. I-III as a function of SNR. As expected, the lowest curve is the one relevant to the strongest (direct) path ($k = 0$) while the other two curves, relative to paths experiencing a single ($k=1$) or a double ($k=2$) reflection, are somewhat shifted versions of the former along the SNR axis, where the shifts are to be ascribed to the different (statistically smaller) path gains. Also to be noted, when the SNR grows, all curves do not decrease indefinitely, but rather they tend asymptotically to different constant (floor) values. This behavior can be explained observing that even though the five signal replicas are sufficiently shifted from one another

as to be substantially uncorrelated, nevertheless they exert a mutual irreducible disturbance whose impact is felt even when the noise vanishes. Accordingly, the different floor levels are related to the different values of signal-to-mutual-interference existing between the signal replicas.

Furthermore, we found that the delay estimates are substantially unbiased for all paths, and this holds true in general provided that the correlation peaks are well separated from one another, i.e., when conditions (21) are met.

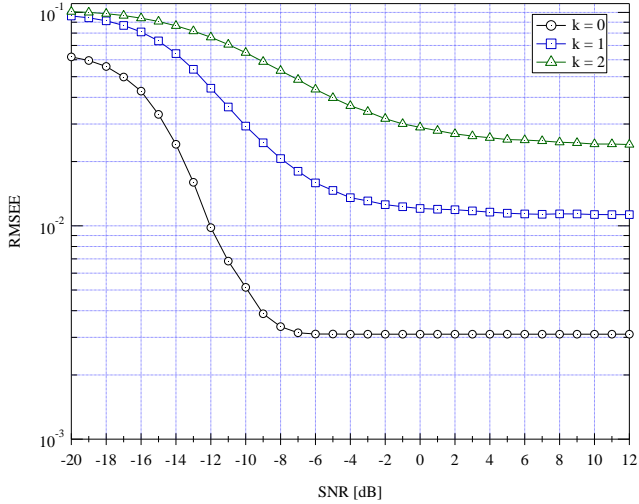


Fig. 9. RMSEE vs SNR, 5-path channel, delay estimate for $k = 0, 1, 2$.

We also assessed the sensitivity of the data detector to residual errors after estimation and compensation of the Doppler-induced distortion on each receiver branch. Indeed, in the presence of relative motion between the transmitter and receiver, the signal replicas received from the channel paths are compressed or expanded in time by the factors $b_k \triangleq \nu_k/c_s$, $k = 1, \dots, K$, where ν_k is the relative speed between the two terminals, and c_s is the sound speed. We note that *i*) this distortion cannot be merely regarded as a frequency shift, in view of the large relative bandwidth occupied by the S2C waveform, entailing different Doppler shifts at the band edges, *ii*) each path undergoes a specific distortion depending on its angle of arrival at the receiver. As noted at the end of Section II, when the above effects cannot be neglected, the receiver must incorporate a block for estimation of the factors b_k and cancellation of the Doppler distortion from each receiver branch. Here we do not focus on any specific algorithm for estimation/cancellation of the Doppler distortion, and limit ourselves to evaluate the sensitivity of the receiver BER to errors in the estimation of the b_k 's. Our aim is to provide a measure of the errors the receiver can tolerate with negligible performance loss and also to compare the behavior of the multiple-branch vs. the single-branch receiver to this specific type of channel impairment. To proceed we let ϵ_k denote the error in the estimation (and subsequent compensation) of b_k for the k -th receiver branch, and model the quantities ϵ_k , $k = 1, \dots, K$ as independent zero-mean Gaussian RVs with equal variance σ_D^2 .

In Fig. 10 we provide some results for the uncoded case, in the form of BER curves vs. SNR obtained in the same

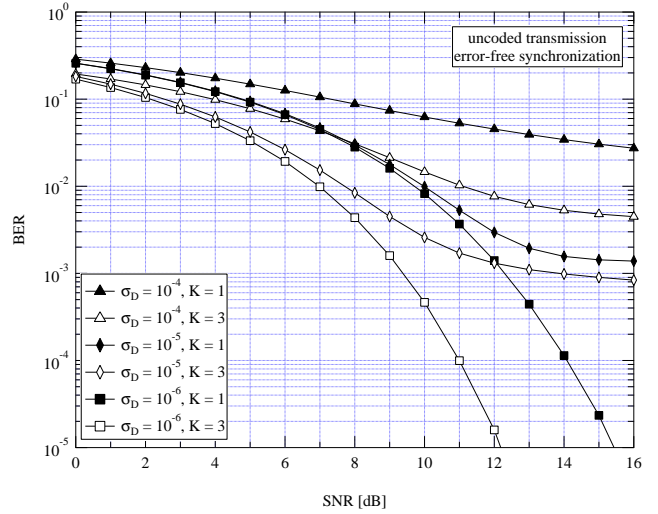


Fig. 10. BER vs SNR with residual Doppler distortion, uncoded transmission, 5-path channel, single-branch and three-branch receivers.

conditions as Fig. 7, except for the presence of the residual Doppler errors ϵ_k on the receiver branches. Similar results were observed for coded transmission. Inspection of the figure reveals that these errors affect the multiple-branch and single-branch receivers approximately in the same way. Specifically, we note that *i*) the impact of residual Doppler distortion is negligible provided that σ_D is around 10^{-6} or smaller, *ii*) larger values of σ_D , say $\sigma_D = 10^{-5}$ or $\sigma_D = 10^{-4}$, progressively degrade the receiver performance and introduce a floor in the BER curves, *iii*) in any case the multiple-branch receiver exhibits a significant edge over the single-branch structure for a given σ_D .

VII. CONCLUSIONS

We have proposed and assessed an alternative implementation of a receiver for S2C transmissions over time-dispersive UWA channels, based on a multiple-branch parallel architecture. Each branch has the task to extract and process the signal received from one of the paths, and the outputs of the branches are finally combined together in an optimal way. We have shown that the above structure is capable to significantly improve the system power efficiency with respect to the classical single-path-based S2C receiver. In particular, we have identified conditions allowing the signal replicas from the various paths to be exactly separated. A real-time version of the system has been implemented on a hardware testbed, and its performance has been assessed in laboratory using typical UWA channel models. For the common situation where in addition to the direct path there are also a few single- or double-bounce reflected paths of nonnegligible level, we have shown that it is possible to achieve power gains of a few decibels in comparison with the single-path receiver. We also discussed an algorithm for synchronization of the despreading signal and for symbol timing recovery, and analyzed its impact on the receiver performance. Finally, we assessed the sensitivity of the multiple-branch receiver to residual Doppler distortion, showing that it still provides a significant margin with respect to the single-branch structure.

REFERENCES

- [1] D.B. Kilfoyle and A.B. Baggeroer, "The state of the art in underwater acoustic telemetry," *IEEE Journal Ocean. Eng.*, vol. 25, no. 1, pp. 4-27, Jan. 2000.
- [2] E.M. Sozer, M. Stojanovic and J.G. Proakis, "Underwater acoustic networks," *IEEE Journal Ocean. Eng.*, vol. 25, no. 1, pp. 72-83, Jan. 2000.
- [3] M. Stojanovic and J. Preisig, "Underwater acoustic communication channels: Propagation models and statistical characterization," *IEEE Commun. Mag.*, vol. 47, no. 1, pp. 84-89, Jan. 2009.
- [4] P.A. van Walree, "Propagation and scattering effects in underwater acoustic communication channels," *IEEE Journal Ocean. Eng.*, vol. 38, no. 4, pp. 614-631, Oct. 2013.
- [5] M. Stojanovic, J.A. Catipovic and J.G. Proakis, "Phase-coherent digital communications for underwater acoustic channels," *IEEE Journal Ocean. Eng.*, vol. 19, no. 1, pp. 100-111, Jan. 1994.
- [6] S. Zhou and Z. Wang, *OFDM for Underwater Acoustic Communications*, Wiley, 2014.
- [7] K.G. Kebkal and R. Bannasch, "Sweep-spread carrier for underwater communication over acoustic channels with strong multipath propagation," *Journal of Acoustical Society of America*, vol.112, n. 5, pp. 2043-2052, Nov. 2002.
- [8] R. Bannasch and K.G. Kebkal, "Method and devices for transmitting and receiving information," US Patent 6,985,749 B2, Jan. 2006.
- [9] K.G. Kebkal, A.K. Kebkal and G.A. Ermolin, "Mathematic and experimental evaluation of phase errors when receiving hydro-acoustic PSK-signals with sweep-spread carrier in reverberant underwater environments," *MTS/IEEE OCEANS'13*, June 10-13 2013, Bergen, pp. 1-8.
- [10] K.G. Kebkal, V.K. Kebkal, O.G. Kebkal and R. Petroccia, "Clock synchronization in underwater acoustic networks during payload data exchange," *2nd International Conference and Exhibition on Underwater Acoustics (UA2014)*, June 22-27 2014, Rhodes, Greece, pp. 1181-1190.
- [11] K.G. Kebkal, A.G. Kebkal and V.K. Kebkal, "Synchronization tools of acoustic communication devices in control of underwater sensors, distributed antennas, and autonomous underwater vehicles," *Gyroscopy and Navigation*, Pleiades Publishing, vol. 5, no. 4, pp. 222-230, 2014.
- [12] J.G. Proakis and M. Salehi, *Digital Communications*, 5th ed., McGraw-Hill, 2007.
- [13] <http://www.ni.com/>
- [14] <http://oalib.hlsresearch.com/>